

H TO ZN IONIZATION EQUILIBRIUM FOR THE NON-MAXWELLIAN ELECTRON κ -DISTRIBUTIONS: UPDATED CALCULATIONS

E. DZIFČÁKOVÁ¹

Astronomical Institute of the Academy of Sciences of the Czech Republic, Fričova 298, 251 65 Ondřejov, Czech Republic

J. DUDÍK¹

Newton International Fellow, DAMTP, CMS, University of Cambridge, Wilberforce Road, Cambridge CB3 0WA, United Kingdom

Draft version March 7, 2022

ABSTRACT

New data for calculation of the ionization and recombination rates have been published in the past few years. Most of these are included in CHIANTI database. We used these data to calculate collisional ionization and recombination rates for the non-Maxwellian κ -distributions with an enhanced number of particles in the high-energy tail, which have been detected in the solar transition region and the solar wind. Ionization equilibria for elements H to Zn are derived. The κ -distributions significantly influence both the ionization and recombination rates and widen the ion abundance peaks. In comparison with Maxwellian distribution, the ion abundance peaks can also be shifted to lower or higher temperatures. The updated ionization equilibrium calculations result in large changes for several ions, notably Fe VIII–XIV. The results are supplied in electronic form compatible with the CHIANTI database.

Keywords: Atomic data – Atomic processes – Radiation mechanisms: non-thermal – Sun: corona – Sun: UV radiation – Sun: X-rays, gamma rays

1. INTRODUCTION

One of the most widely used assumptions in the interpretation of astrophysical spectra is that the emitting system is in thermal equilibrium. This means that the distribution of particle energies is at least locally Maxwellian, and can be characterized by the Boltzmann-Gibbs statistics which has one parameter, the temperature.

The generalization of the Boltzmann-Gibbs statistics proposed by Tsallis (1988, 2009), results in κ -distributions (e.g., Leubner 2002, 2004a,b; Collier 2004; Livadiotis & McComas 2009), characterized by a parameter κ and exhibiting a near-Maxwellian core and a high-energy power-law tail (Sect. 2). First proposed by Vasyliunas (1968), the κ distributions are now used to fit the observations of a wide variety of astrophysical environments, e.g. in-situ measurements of particle distributions in planetary magnetic environments (e.g., Pierrard & Lemaire 1996; Mauk et al. 2004; Schippers et al. 2008; Xiao et al. 2008; Dialynas et al. 2009) and solar wind (e.g., Collier et al. 1996; Maksimovic et al. 1997a,b; Pierrard et al. 1999; Nieves-Chinchilla & Viñas 2008; Le Chat et al. 2009, 2011; Pierrard 2012), as well as photon spectra of solar flare plasmas (e.g., Kašparová & Karlický 2009; Oka et al. 2013), emission line spectra of planetary nebulae and galactic sources (Nicholls et al. 2012; see also Binette et al. 2012) and even solar transition region (Dzifčáková et al. 2011). A review on the κ -distributions and their applications in astrophysical plasma can be found, e.g., in Pierrard & Lazar (2010).

In the solar corona, presence of the κ -distributions, or distributions exhibiting high-energy tails, can be expected due to particle acceleration processes arising as a result of “nanoflare” heating. The nanoflares are an unknown energy release process of impulsive nature, occurring possibly in storms heating the solar corona (e.g., Tripathi et al. 2010; Viall & Klimchuk 2011; Bradshaw et al. 2012; Winebarger 2012). While the direct evidence for enhanced suprathermal populations in the solar corona is still lacking (Feldman et al. 2007; Hannah et al. 2010), Pinfield et al. (1999) reported that the intensities of the Si III transition region lines observed by the SOHO/SUMER instrument do not correspond to a single Maxwellian distribution. Using their data, Dzifčáková & Kulinová (2011) showed that the observed intensities can be explained by κ -distributions once the photoexcitation is taken into account. These authors diagnosed $\kappa = 7$ in the active region observed on the solar limb. Higher values of κ were diagnosed for the quiet Sun and coronal hole, indicating that the departures from the Maxwellian distribution can be connected to the local magnetic activity. The diagnostic method also works for inhomogeneous plasmas characterized by differential emission measure. That the κ -distributions can be present in the solar corona is also suggested by their presence in the solar wind (e.g., Pierrard et al. 1999; Vocks & Mann 2003).

Direct diagnostics of κ -distributions in the solar corona using extreme-ultraviolet lines observed by the Hinode/EIS spectrometer (Culhane et al. 2007) were attempted by Dzifčáková & Kulinová (2010) and Mackovjak et al. (2013). These authors proposed methods for simultaneous diagnostics of the plasma temperature, electron density, and κ . However, majority of the line ratios sensitive to κ -distributions suffer from poor

elena@asu.cas.cz

¹DAPEM, Faculty of Mathematics Physics and Computer Science, Comenius University, Mlynská Dolina F2, 842 48 Bratislava, Slovakia

photon statistics, errors in atomic data and/or plasma inhomogeneities. In spite of this, one of the main results of these works is that the sensitivity to κ -distributions, or to departures from the Maxwellian distribution in general, is enhanced if the line ratios involve lines originating in neighboring ionization stages. This is due the sensitivity of the line emissivity to the abundance of the emitting ion that depends directly on the ionization equilibrium in turn highly dependent on the type of the distribution (e.g., Dzifčáková 2002; Wannawichian et al. 2003; Dzifčáková 2006).

In the past decade, new calculations of the ionization, recombination rates and ionization equilibrium for the Maxwellian electron distribution were published. These are summarized in the continually updated CHIANTI database, currently available in version 7.1 (e.g., Dere et al. 1997, 2009; Landi et al. 2012, 2013). These new calculations of the ionization and recombination rates result in significant differences with respect to the earlier calculations, e.g. of Mazzotta et al. (1998).

The availability of accurate atomic data are of crucial importance in correct determination of the properties of the radiating astrophysical environment, and the solar corona in particular. In this paper, we present up-to-date calculations of the ionization and recombination rates (Sect. 3), and ionization equilibria (Sect. 4) for κ -distributions for elements from H to Zn. Such calculations are necessary for diagnostics of the κ -distributions in both the solar transition region and the corona, as well as subsequent calculations of the radiative losses (Dudík et al. 2011) or responses of various extreme-ultraviolet or X-ray filters (Dudík et al. 2009) used both to model and observe these portions of the solar atmosphere, with potential applications to other astrophysical environments.

2. THE NON-MAXWELLIAN κ -DISTRIBUTIONS

The κ -distributions of electron kinetic energies \mathcal{E} represent a family of non-Maxwellian distributions characterized by two parameters, κ and T

$$f_{\kappa}(\mathcal{E})d\mathcal{E} = \mathcal{A}_{\kappa} \frac{2}{\pi^{1/2}(k_{\text{B}}T)^{3/2}} \frac{\mathcal{E}^{1/2}d\mathcal{E}}{\left(1 + \frac{\mathcal{E}}{(\kappa-1.5)kT}\right)^{\kappa+1}}, \quad (1)$$

where the $\mathcal{A}_{\kappa} = \Gamma(\kappa+1)/[\Gamma(\kappa-0.5)(\kappa-1.5)^{3/2}]$ is the normalization constant, $k_{\text{B}} = 1.38 \times 10^{-23} \text{ J kg}^{-1}$ is the Boltzmann constant, and $\kappa \in (3/2, +\infty)$, $T \in (0, +\infty)$. We note that the definition of κ -distributions in Eq. (1 *top*) corresponds to the κ -distributions of the second kind (e.g., Livadiotis & McComas 2009).

The shape of the distribution is controlled by the parameter κ . Maxwellian distribution is recovered for $\kappa \rightarrow +\infty$, while the departures from the Maxwellian increase with $\kappa \rightarrow 3/2$. The departures from the Maxwellian distribution with decreasing κ include increase of the number of particles in the high-energy tail as well as increase in the relative number of low-energy electrons (Fig. 1 *top*). However, the mean energy $\langle \mathcal{E} \rangle = 3/2k_{\text{B}}T$ of the distribution does not depend on κ . This allows for calculation of all quantities depending on the mean energy of the distribution, e.g. pressure (Dzifčáková 2006). The parameter T has in the frame of nonextensive statistics (Tsallis 1988, 2009) an analogous meaning as thermodynamic temperature in the

Boltzmann-Gibbs statistics. The reader is referred e.g. to the work of Livadiotis & McComas (2009, 2010) for details.

While the shape of the κ -distribution differs from the Maxwellian with the same T at all energies E , the core of the κ -distribution can be approximated by a Maxwellian distribution with lower $T_{\text{C}} = T(\kappa - 3/2)/\kappa$ (Oka et al. 2013). An example for $\kappa = 5$ and $T = 1 \text{ MK}$ is shown in Fig. 1 *bottom*, where the approximating Maxwellian distribution has $T_{\text{C}} = 0.7T$ and has been scaled by the factor C

$$C = 2.718 \frac{\Gamma(\kappa+1)}{\Gamma(\kappa-1/2)} \kappa^{-3/2} \left(1 + \frac{1}{\kappa}\right)^{-(\kappa+1)} \quad (2)$$

(Oka et al. 2013), which is ≈ 0.84 for $\kappa = 5$. The difference between the $f_{\kappa}(T)$ and $f_{\text{Maxw}}(T_{\text{C}})$ are then mainly in the pronounced high-energy tail. This shows that the κ distributions offer straightforward approximation of situations where a non-Maxwellian high-energy tail is present.

3. IONIZATION AND RECOMBINATION RATES

To calculate the ionization and recombination rates for κ -distributions, we use the atomic data available through the CHIANTI database for astrophysical spectroscopy of optically thin plasmas (Dere et al. 1997; Landi et al. 2013). The analytical functional form of the κ -distributions allows for relatively simple direct integration of the ionization cross-sections (Sect 3.2). However, the recombination cross-sections are not contained in CHIANTI. These then have to be reverse-engineered from the Maxwellian recombination rates using assumptions detailed in Sect. 3.3.

We note that the CHIANTI database allows for the treatment of non-Maxwellian distributions only if these can be represented by a series of individual Maxwellian distributions (with different T s). The technique for calculation of ionization and recombination rates presented here can in principle be extended for any type of particle distribution, not only κ -distributions.

3.1. Atomic Data

The CHIANTI atomic database since version 6 (Dere et al. 2009) contains continually updated ionization equilibrium for the Maxwellian distribution. This ionization equilibrium utilizes the cross-sections for direct ionization and autoionization, and the corresponding rate coefficients from the work of Dere (2007). Dielectronic and radiative recombination coefficients for the H to Al and Ar isoelectronic sequences are taken from the works of N. Badnell and colleagues, listed at <http://amdpp.phys.strath.ac.uk/tamoc/DATA/> (Badnell et al. 2003; Colgan et al. 2003, 2004; Mitnik & Badnell 2004; Badnell 2006; Altun et al. 2005, 2006, 2007; Zatsarinny et al. 2005a,b, 2006; Bautista & Badnell 2007; Nikolić et al. 2010; Abdel-Naby et al. 2012). For the Si to Mn isoelectronic sequences, the recombination rates are based on the works of Shull & van Steenberg (1982), Nahar (1996, 1997), Nahar & Bautista (2001), Mazzotta et al. (1998) and Mazzitelli & Mattioli (2002). The reader is referred to Dere et al. (2009) for details. In the calculations presented in this paper, all atomic data for

ionization and recombination correspond to the ones used to produce the *chianti.ioneq* file in the CHIANTI v7.1. We note that ionization equilibria were published also by other authors (e.g. Bryans et al. 2009), but these use mostly the same atomic data as the CHIANTI database.

3.2. Ionization Rates

The ionization rates have been calculated by a numerical integration of the ionization cross section, σ_i , available in CHIANTI database

$$R_i = \langle \sigma_i v \rangle = \int_0^\infty \sigma_i \left(\frac{2\mathcal{E}}{m} \right)^{1/2} f_\kappa(\mathcal{E}) d\mathcal{E}, \quad (3)$$

for $\kappa = 2, 3, 5, 7, 10, 25$, and 33 . Each numerical integral is calculated as a sum of individual integrals splitted according to the ionization and auto-ionization energies.

Typical changes in behaviour of the direct ionization and autoionization rates with κ -distributions are shown in Fig. 2 for the ions C IV, Fe XII, and Fe XVII formed at transition region, quiet coronal, and flare conditions, respectively. For lower κ , the temperature dependence of the ionization rates is much flatter, with lower maxima. Typically, for temperatures lower than those at which the ion abundance peaks (denoted by arrow in Fig. 2, see also Sect. 4), the κ -distributions result in increase of the ionization rates by up to several orders of magnitude with respect to the Maxwellian distribution. These deviations from Maxwellian ionization rates increase with decreasing κ .

3.3. Recombination Rates

Since the individual recombination cross-sections are not available in CHIANTI, the calculation of the recombination rates for κ -distributions was performed using the method of Dzifčáková (1992), used also by Wannawichian et al. (2003). This method allows for calculation of the recombination rates using approximations to the rates for the Maxwellian distribution.

The cross-section σ_{RR} for the radiative recombination is assumed to have a power-law dependence on energy (Osterbrock 1974)

$$\sigma_{RR}(\mathcal{E}) = C_{RR}/\mathcal{E}^{\eta+0.5}, \quad (4)$$

where C_{RR} is a constant and $\eta+0.5$ is a power-law index. Subsequently, the radiative recombination rate for the κ -distribution is of the form:

$$R_{RR}^\kappa = \frac{4C_{RR}}{(2\pi m)^{1/2}} \frac{\Gamma(\kappa + \eta - 0.5)(\kappa - 1.5)^\eta \Gamma(1.5 - \eta)}{\Gamma(\kappa - 0.5) (k_B T)^\eta}, \quad (5)$$

while the radiative recombination rate for the Maxwellian distribution is

$$R_{RR}^{\text{Maxw}} = \frac{4C_{RR}}{(2\pi m)^{1/2}} \frac{\Gamma(1.5 - \eta)}{(k_B T)^\eta}. \quad (6)$$

Therefore, it holds that

$$R_{RR}^\kappa = R_{RR}^{\text{Maxw}} \frac{\Gamma(\kappa + \eta - 0.5)(\kappa - 1.5)^\eta}{\Gamma(\kappa - 0.5)}. \quad (7)$$

The level of error introduced by this approximation is typically several per cent, i.e., lower than the error of the atomic data themselves.

For the dielectronic recombination, following approximation has been taken (Dzifčáková 1992)

$$R_{DR}^\kappa = \frac{A_\kappa}{T^{1/3}} \sum_i \frac{a_i}{(1 + t_i/(\kappa - 1.5)T)^{(\kappa+1)}}, \quad (8)$$

where parameters a_i and t_i are the same as in similar expressions for the Maxwellian distribution

$$R_{DR}^{\text{Maxw}} = \frac{1}{T^{1/3}} \sum_i a_i \exp(-t_i/T), \quad (9)$$

where the coefficients a_i and t_i are provided within the CHIANTI database. The precision of this approximation is given by the magnitude of the second-order terms in the expansion of the coefficients a_i and t_i into series (Eqs. 37–44 in Dzifčáková 1992).

The typical behavior of the total recombination rates ($R_{RR} + R_{DR}$) for κ -distributions and for Maxwellian distribution is shown in Fig. 2. It can be seen that the radiative recombination rate increases with decrease of κ . This is a result of increasing number of low energy electrons for the κ -distributions (Fig. 1), which dominate the recombination processes. The local change of slope of total recombination rate is caused by the contribution of dielectronic recombination. For some ions, e.g. Fe XVII, the contribution of dielectronic recombination is dominant in temperature interval where these ions have a non-negligible abundance.

4. THE IONIZATION EQUILIBRIUM

Calculations of the collisional ionization equilibrium assume that there are no temporal variations in plasma temperature T . In the coronal conditions, the resulting relative ion populations are given by the equilibrium between the direct collisional ionization with auto-ionization and the radiative and dielectronic recombination. Three-body processes can be neglected at low electron densities typical in the solar corona (Phillips et al. 2008). The radiative field is also usually assumed to be too weak, i.e., photoionization can be neglected as well. However, we note that photoionization may be important for some transition-region ions with low ionization thresholds, but the effect will vary depending on the distance from the radiation field (e.g., the solar photosphere).

The ionization equilibrium for κ -distributions with $\kappa = 2, 3, 5, 7, 10, 25$, and 33 was calculated for ions of astrophysical interests, ranging from H ($Z=1$) to Zn ($Z=30$). Previous calculations of Dzifčáková (1992), Dzifčáková (2002), and Wannawichian et al. (2003) involved only 12 most abundant elements. The current calculations are performed for the same set of temperatures as the calculations in the CHIANTI database in the *chianti.ioneq* file. I.e., the temperature spans the interval of $\log(T/\text{K}) \in \langle 4, 9 \rangle$ with the step of $\Delta \log(T/\text{K}) = 0.05$. The calculations are available in the same format as the *chianti.ioneq* file and are easily readable using the routines *read_ioneq.pro* and *plot_ioneq.pro* available in CHIANTI running under SolarSoftware in IDL. More information on the CHIANTI *ioneq* file format is provided in Appendix A.

Examples of the current ionization equilibrium calculations for iron are in Fig. 3 and for carbon in

Fig. 4. The typical behavior is that the lower κ , the flatter the ionization peaks. In addition, ionization peaks can be shifted to lower or higher T , depending on κ , T and the individual ion. This means that a given relative ion abundance can be formed at a wider range of T for a κ -distribution, with different peak formation temperature. Such behavior was already reported by Dzifčáková (1992), Dzifčáková (2002) and Wannawichian et al. (2003). Typically, the shifts of Fe and C ion abundance peaks are to lower T with respect to the Maxwellian ionization equilibrium if $\log(T/K) \lesssim 5.5$. At coronal temperatures, the Fe IX – Fe XVI ions are shifted to higher T . An interesting example is the ion Fe XVII, whose ionization peak is shifted to lower T for $\kappa \text{ lessapprox } 3$, but to higher T for $\kappa = 2$ (Fig. 3 *bottom*).

There are a number of differences with respect to the earlier calculations of Dzifčáková (2002), which used the atomic data corresponding to those of Mazzotta et al. (1998). These differences are illustrated in Fig. 5. In general, the lower the value of κ , the greater the differences with respect to the previous calculations. The most conspicuous examples are the Fe IX, which is shifted to slightly higher T instead to lower T as in the previous calculations of Dzifčáková (2002). The Fe XII and Fe XIII ions are shifted to higher T (up to 0.1–0.15 dex). We note that the changes in the ionization equilibria due to the updated atomic data will reflect e.g. on changes in the total radiative losses (Dudík et al. 2011) and will also modify the proposed diagnostic methods for κ -distributions (Dzifčáková & Kulinová 2010; Mackovjak et al. 2013).

Ratios of relative abundances of individual ions can be used to diagnose the value of κ and simultaneously T . Such diagnostics can be applied e.g. in the solar wind (Owocki & Scudder 1983). An example of diagnostic diagrams is given in Fig. 6. We note that such diagrams cannot be directly applied on the observed line intensities unless the additional effect of κ -distributions on the excitation and deexcitation rates is considered. However, these diagrams provide quantification of the expected changes to ratios of line intensities due to ionization equilibrium. Ratios of lines involving different ionization stages provide better options for determining κ , as noted already by (Dzifčáková & Kulinová 2010; Mackovjak et al. 2013).

5. SUMMARY

Collisional ionization equilibrium calculations for κ -distributions and optically thin plasmas were performed for all ions of elements H to Zn. To do that, the latest available atomic data for ionization and recombination were used. The calculations are available in the form of ionization equilibrium files compatible with the CHIANTI database, v7.1.

For κ -distributions, the ionization peaks are in general flatter and can be shifted to lower or higher T . This means that for κ -distributions, individual ions are typically formed in a wider range of temperatures, with different peak formation temperatures. Typically, ions formed at transition region temperatures are shifted to lower T , while the majority of coronal iron ions are shifted to higher T . Comparison to previous calculations is provided. Due to updated atomic data calculations, several ions in the present calculations are shifted to different temperatures with respect to previous calculations of Dzifčáková (2002). The effect of κ on the ratios of ion abundances is documented.

The present calculations provide an accurate, necessary and useful tool for detection of astrophysical plasmas out of thermal equilibrium, where the distribution of particles is characterized by an enhanced power-law tail. The supplied files compatible with the CHIANTI database and software should greatly facilitate synthesis of both line and continuum spectra for optically thin astrophysical plasmas.

The authors are grateful to Dr. G. Del Zanna and Dr. H. E. Mason for helpful discussions. This work was supported by Grant Agency of the Czech Republic, Grant No. P209/12/1652, the project RVO:67985815, Scientific Grant Agency, VEGA, Slovakia, Grant No. 1/0240/11, and the bilateral project APVV CZ-SK-0153-11 (7AMB12SK154) involving the Slovak Research and Development Agency and the Ministry of Education of the Czech Republic. JD acknowledges support from the Comenius University Grant No. UK/11/2012. CHIANTI is a collaborative project involving the NRL (USA), RAL (UK), MSSL (UK), the Universities of Florence (Italy) and Cambridge (UK), and George Mason University (USA). CHIANTI is great spectroscopic database and software, and the authors are very grateful for its existence and availability.

APPENDIX

CHIANTI .IONEQ FILE FORMAT

The *.ioneq* files, used by the CHIANTI database and software to store data on the ionization equilibrium, are in essence formatted ASCII files. An example of their format is given in Table 1. The file begins with two numbers, N , giving the number of temperature points T_i , $1 \leq i \leq N$, and Z_{\max} , denoting the maximum proton number Z for which the ionization equilibrium is provided. The next line gives the tabulated temperatures $\log(T_i/K)$. All other following lines begin with the Z and a positive integer $+k$ denoting the roman numeral for the corresponding ion; e.g., 26 and 9 stands for Fe IX. The line then contains relative ion abundances $A_Z^{+k-1}(T_i)$ in floating-point precision for the tabulated temperatures.

Portion of the actual content of the *kappa_05.ioneq* file is given in Table 2. There, the relative abundances of the ions Fe IX–Fe XI are listed for $\kappa = 5$ and for $\log(T/K) = 5.80 - 6.15$.

Table 2

Example of the *kappa_05.ioneq* file produced for $\kappa = 5$. The table shows relative abundances of the ions Fe IX – Fe XI.

101	30	...	5.80	5.85	5.90	5.95	6.00	6.05	6.10	6.15	...
...
26
26	9	...	0.357000	0.405000	0.422800	0.401500	0.342300	0.257800	0.167600	0.091260	...
26	10	...	0.0905900	0.144700	0.211400	0.279200	0.329100	0.340500	0.302200	0.223100	...
26	11	...	0.00983700	0.0228500	0.0481900	0.0912400	0.153000	0.223400	0.277700	0.284900	...
26
...

REFERENCES

- Abdel-Naby, S. A., Nikolić, D., Gorczyca, T. W., Korista, K. T., & Badnell, N. R. 2012, *A&A*, 537, A40
- Altun, Z., Yumak, A., Badnell, N. R., Colgan, J., & Pindzola, M. S. 2005, *A&A*, 433, 395
- Altun, Z., Yumak, A., Badnell, N. R., Loch, S. D., & Pindzola, M. S. 2006, *A&A*, 447, 1165
- Altun, Z., Yumak, A., Yavuz, I., et al. 2007, *A&A*, 474, 1051
- Badnell, N. R. 2006, *A&A*, 447, 389
- Badnell, N. R., O’Mullane, M. G., Summers, H. P., et al. 2003, *A&A*, 406, 1151
- Bautista, M. A., & Badnell, N. R. 2007, *A&A*, 466, 755
- Binette, L., Matadamas, R., Hägele, G. F., et al. 2012, *A&A*, 547, A29
- Bradshaw, S. J., Klimchuk, J. A., & Reep, J. W. 2012, *ApJ*, 758, 53
- Bryans, P., Landi, E., & Savin, D. W. 2009, *ApJ*, 691, 1540
- Colgan, J., Pindzola, M. S., & Badnell, N. R. 2004, *A&A*, 417, 1183
- Colgan, J., Pindzola, M. S., Whiteford, A. D., & Badnell, N. R. 2003, *A&A*, 412, 597
- Collier, M. R. 2004, *Advances in Space Research*, 33, 2108
- Collier, M. R., Hamilton, D. C., Gloeckler, G., Bochsler, P., & Sheldon, R. B. 1996, *Geophys. Res. Lett.*, 23, 1191
- Culhane, J. L., Harra, L. K., James, A. M., et al. 2007, *Sol. Phys.*, 243, 19
- Dere, K. P. 2007, *A&A*, 466, 771
- Dere, K. P., Landi, E., Mason, H. E., Monsignori Fossi, B. C., & Young, P. R. 1997, *A&AS*, 125, 149
- Dere, K. P., Landi, E., Young, P. R., et al. 2009, *A&A*, 498, 915
- Dialynas, K., Krimigis, S. M., Mitchell, D. G., et al. 2009, *J. Geophys. Res.*, 114, A01212
- Dudík, J., Dzifčáková, E., Karlický, M., & Kulinová, A. 2011, *A&A*, 529, A103
- Dudík, J., Kulinová, A., Dzifčáková, E., & Karlický, M. 2009, *A&A*, 505, 1255
- Dzifčáková, E. 2002, *Sol. Phys.*, 208, 91
- . 2006, *Sol. Phys.*, 234, 243
- Dzifčáková, E., Homola, M., & Dudík, J. 2011, *A&A*, 531, A111
- Dzifčáková, E., & Kulinová, A. 2010, *Sol. Phys.*, 263, 25
- . 2011, *A&A*, 531, A122
- Dzifčáková, E. 1992, *Sol. Phys.*, 140, 247
- Feldman, U., Landi, E., & Doschek, G. A. 2007, *ApJ*, 660, 1674
- Hannah, I. G., Hudson, H. S., Hurford, G. J., & Lin, R. P. 2010, *ApJ*, 724, 487
- Kašparová, J., & Karlický, M. 2009, *A&A*, 497, L13
- Landi, E., Del Zanna, G., Young, P. R., Dere, K. P., & Mason, H. E. 2012, *ApJ*, 744, 99
- Landi, E., Young, P. R., Dere, K. P., Del Zanna, G., & Mason, H. E. 2013, *ApJ*, submitted
- Le Chat, G., Issautier, K., Meyer-Vernet, N., & Hoang, S. 2011, *Sol. Phys.*, 271, 141
- Le Chat, G., Issautier, K., Meyer-Vernet, N., et al. 2009, *Physics of Plasmas*, 16, 102903
- Leubner, M. P. 2002, *Ap&SS*, 282, 573
- . 2004a, *ApJ*, 604, 469
- . 2004b, *Physics of Plasmas*, 11, 1308
- Livadiotis, G., & McComas, D. J. 2009, *J. Geophys. Res.*, 114, A11105
- . 2010, *ApJ*, 714, 971
- Mackovjak, Š., Dzifčáková, E., & Dudík, J. 2013, *Sol. Phys.*, 282, 263
- Maksimovic, M., Pierrard, V., & Lemaire, J. F. 1997a, *A&A*, 324, 725
- Maksimovic, M., Pierrard, V., & Riley, P. 1997b, *Geophys. Res. Lett.*, 24, 1151
- Mauk, B. H., Mitchell, D. G., McEntire, R. W., et al. 2004, *J. Geophys. Res.*, 109, A09S12
- Mazzitelli, G., & Mattioli, M. 2002, *Atomic Data and Nuclear Data Tables*, 82, 313
- Mazzotta, P., Mazzitelli, G., Colafrancesco, S., & Vittorio, N. 1998, *A&AS*, 133, 403
- Mitnik, D. M., & Badnell, N. R. 2004, *A&A*, 425, 1153
- Nahar, S. N. 1996, *Phys. Rev. A*, 53, 2417
- . 1997, *Phys. Rev. A*, 55, 1980
- Nahar, S. N., & Bautista, M. A. 2001, *ApJS*, 137, 201
- Nicholls, D. C., Dopita, M. A., & Sutherland, R. S. 2012, *ApJ*, 752, 148
- Nieves-Chinchilla, T., & Viñas, A. F. 2008, *J. Geophys. Res.*, 113, A02105
- Nikolić, D., Gorczyca, T. W., Korista, K. T., & Badnell, N. R. 2010, *A&A*, 516, A97
- Oka, M., Ishikawa, S., Saint-Hilaire, P., Krucker, S., & Lin, R. P. 2013, *ApJ*, 764, 6
- Osterbrock, D. E. 1974, *Astrophysics of gaseous nebulae*
- Owoccki, S. P., & Scudder, J. D. 1983, *ApJ*, 270, 758
- Phillips, K. J. H., Feldman, U., & Landi, E. 2008, *Ultraviolet and X-ray Spectroscopy of the Solar Atmosphere* (Cambridge University Press)
- Pierrard, V. 2012, *Space Sci. Rev.*, 172, 315
- Pierrard, V., & Lazar, M. 2010, *Sol. Phys.*, 267, 153
- Pierrard, V., & Lemaire, J. 1996, *J. Geophys. Res.*, 101, 7923
- Pierrard, V., Maksimovic, M., & Lemaire, J. 1999, *J. Geophys. Res.*, 104, 17021
- Pinfield, D. J., Keenan, F. P., Mathioudakis, M., et al. 1999, *ApJ*, 527, 1000
- Schippers, P., Blanc, M., André, N., et al. 2008, *J. Geophys. Res.*, 113, A07208
- Shull, J. M., & van Steenberg, M. 1982, *ApJS*, 48, 95
- Tripathi, D., Mason, H. E., & Klimchuk, J. A. 2010, *ApJ*, 723, 713
- Tsallis, C. 1988, *Journal of Statistical Physics*, 52, 479
- . 2009, *Introduction to Nonextensive Statistical Mechanics* (Springer New York, 2009)
- Vasyliunas, V. M. 1968, in *Astrophysics and Space Science Library*, Vol. 10, *Physics of the Magnetosphere*, ed. R. D. L. Carovillano & J. F. McClay, 622
- Vial, N. M., & Klimchuk, J. A. 2011, *ApJ*, 738, 24
- Vocks, C., & Mann, G. 2003, *ApJ*, 593, 1134
- Wannawichian, S., Ruffolo, D., & Kartavykh, Y. Y. 2003, *ApJS*, 146, 443
- Winebarger, A. R. 2012, in *Astronomical Society of the Pacific Conference Series*, Vol. 456, *Fifth Hinode Science Meeting*, ed. L. Golub, I. De Moortel, & T. Shimizu, 103
- Xiao, F., Shen, C., Wang, Y., Zheng, H., & Wang, S. 2008, *Journal of Geophysical Research* (Space Physics), 113, 5203
- Zatsarinny, O., Gorczyca, T. W., Fu, J., et al. 2006, *A&A*, 447, 379
- Zatsarinny, O., Gorczyca, T. W., Korista, K. T., et al. 2005a, *A&A*, 438, 743
- . 2005b, *A&A*, 440, 1203

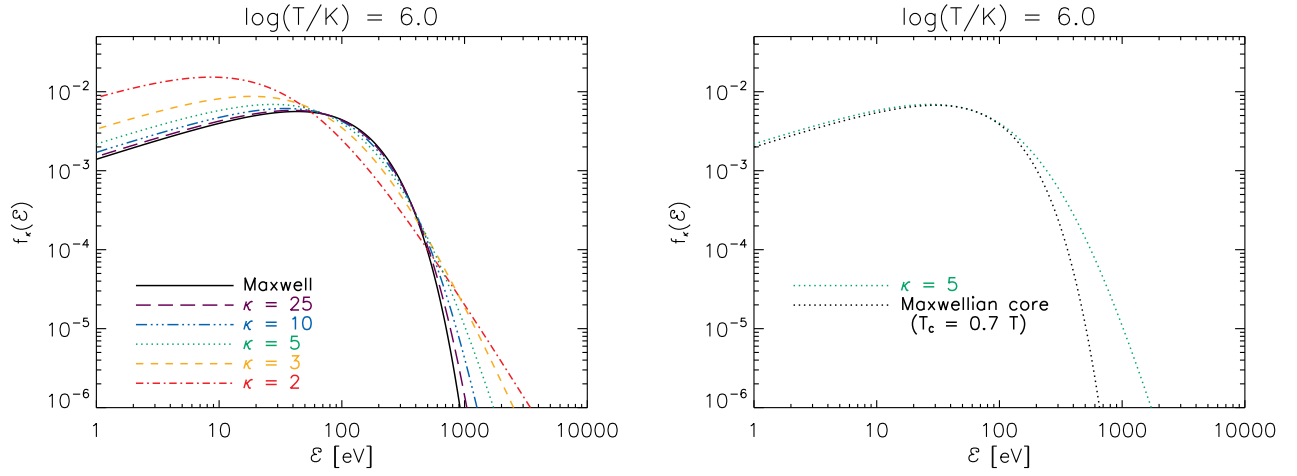


Figure 1. *Top:* The κ -distributions with $\kappa = 2, 3, 5, 10, 25$ and the Maxwellian distribution plotted for $\log(T/K) = 6.0$. *Bottom:* The $\kappa = 5$ distribution and the approximation of its core with Maxwellian distribution with lower T_C . Colors and linestyles correspond to different values of κ . (A color version of this figure is available in the online journal.)

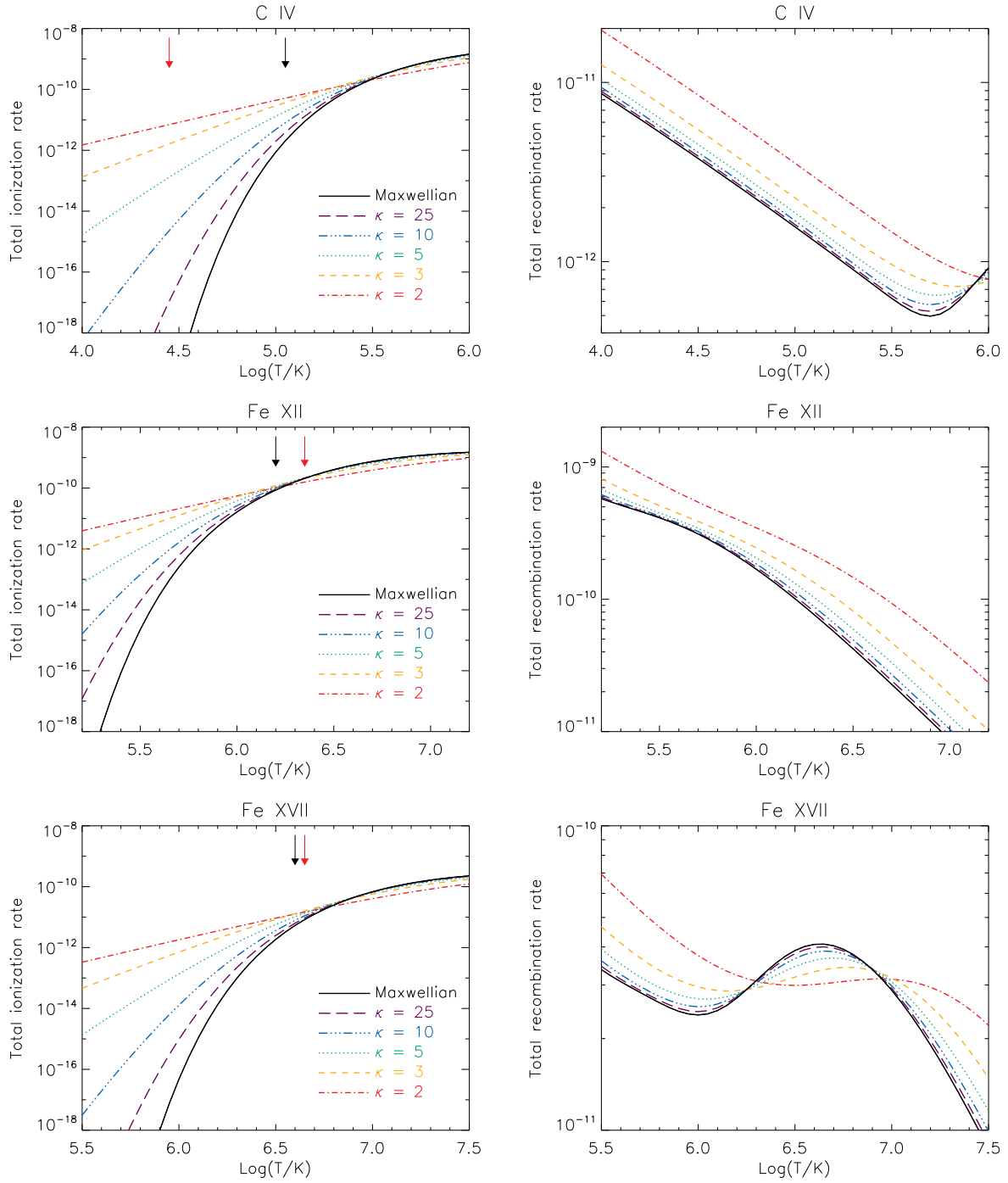


Figure 2. Total ionization and recombination rates for C IV (*top row*), Fe XII (*middle row*) and Fe XVII (*bottom row*). Different linestyles correspond to different κ . Black and red arrows denote maximum of the relative ion abundance for the Maxwellian and $\kappa = 2$ distributions, respectively. (A color version of this figure is available in the online journal.)

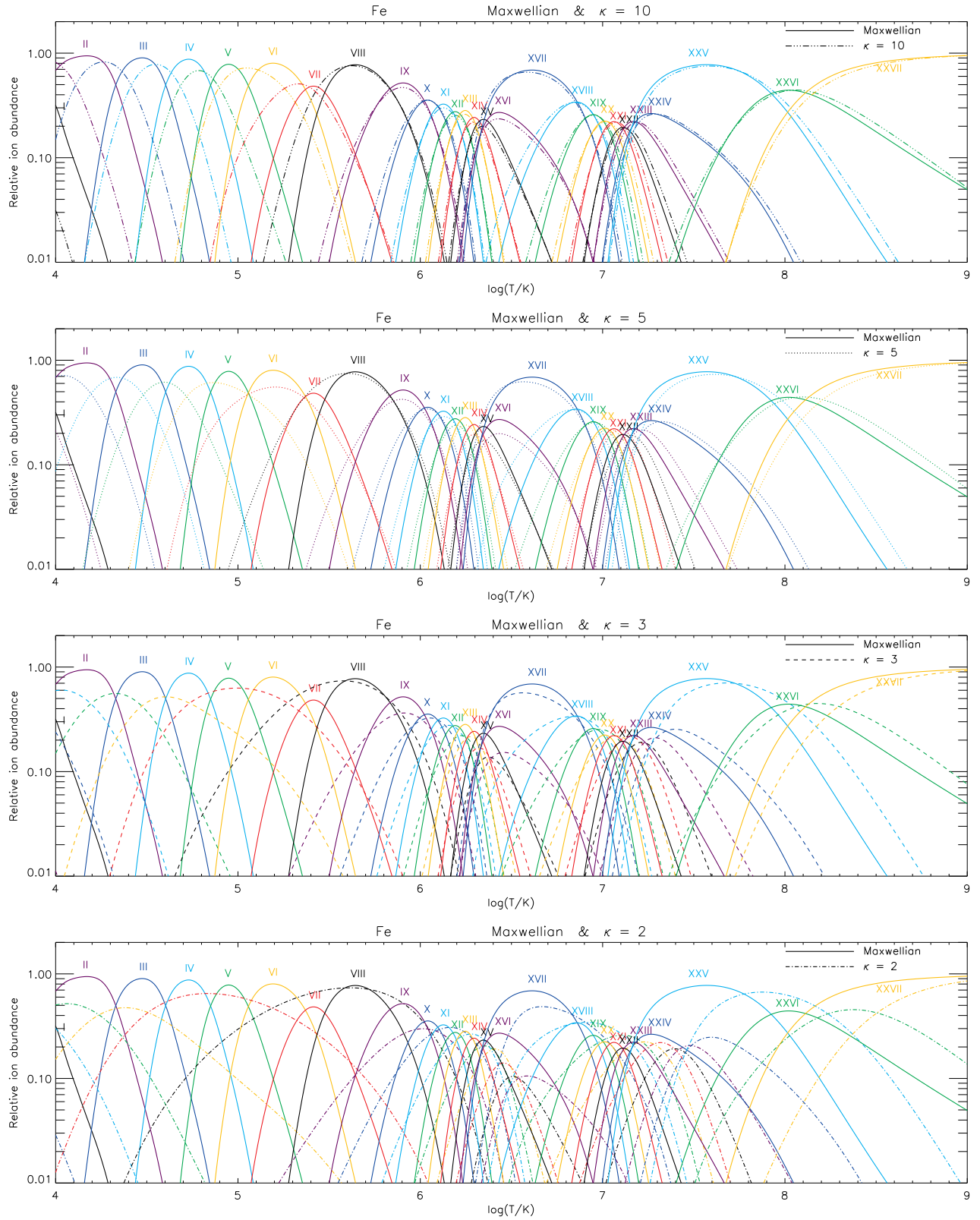


Figure 3. Changes in the ionization equilibrium with κ for iron. *Top:* $\kappa = 10$; *Second row:* $\kappa = 5$; *Third row:* $\kappa = 5$; *Bottom row:* $\kappa = 2$. Individual ionization stages are indicated. (A color version of this figure is available in the online journal.)

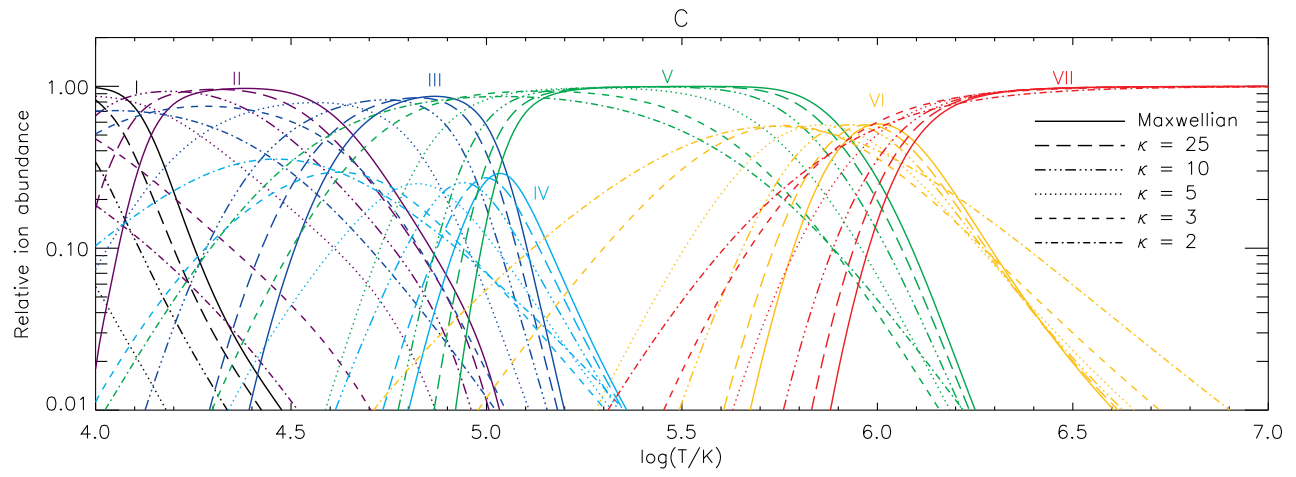


Figure 4. Ionization equilibrium for Carbon. Different linestyles correspond to different κ . (A color version of this figure is available in the online journal.)

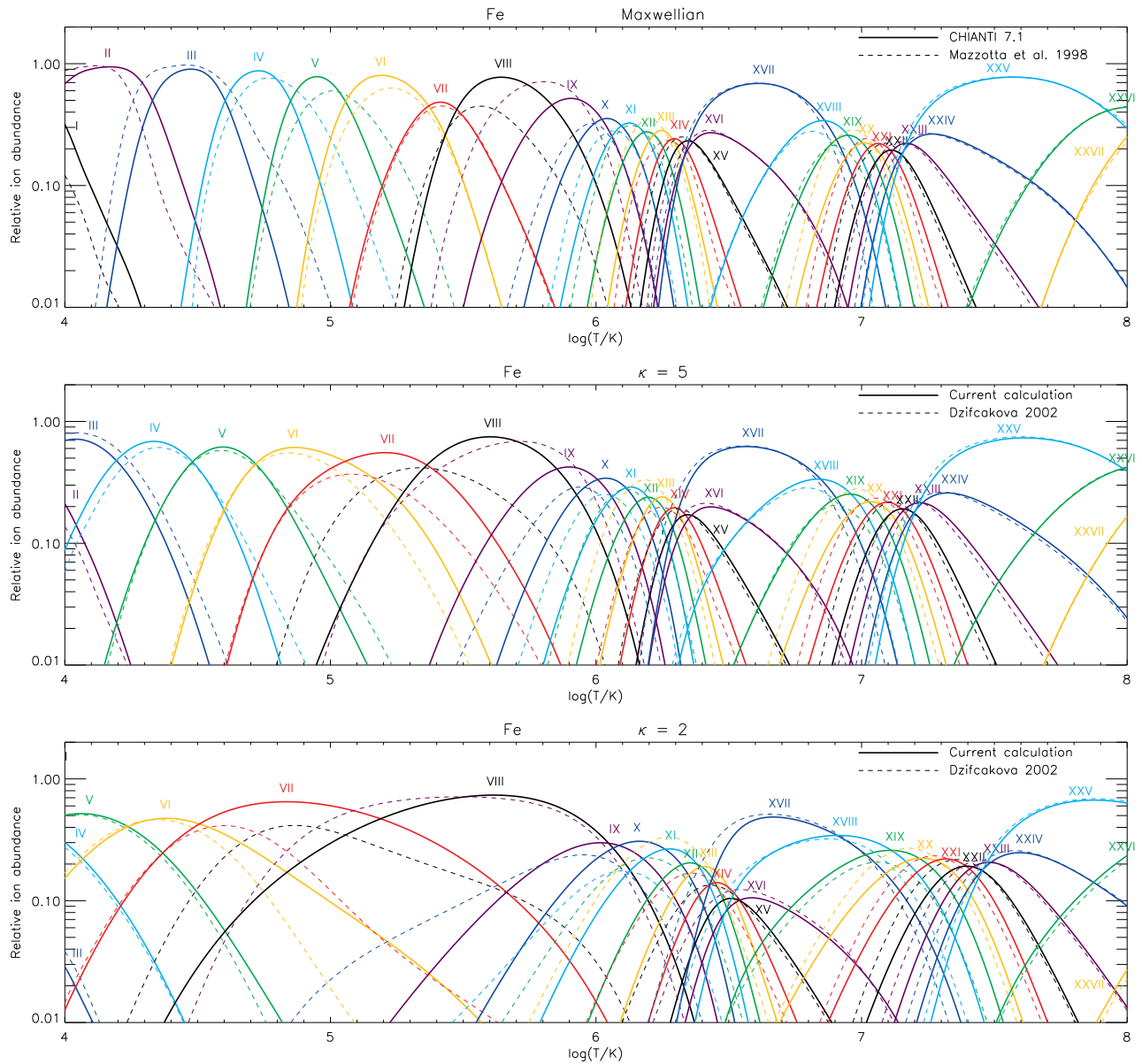


Figure 5. Comparison of the current, updated calculations with the previous ones. *Top:* Comparison between the ionization equilibrium according to Dere et al. (2009) and Mazzotta et al. (1998). *Middle and Bottom:* Comparison of the current calculations with the ones of Dzifčáková (2002) for $\kappa=5$ and 2, respectively. Individual ionization stages are indicated. (A color version of this figure is available in the online journal.)

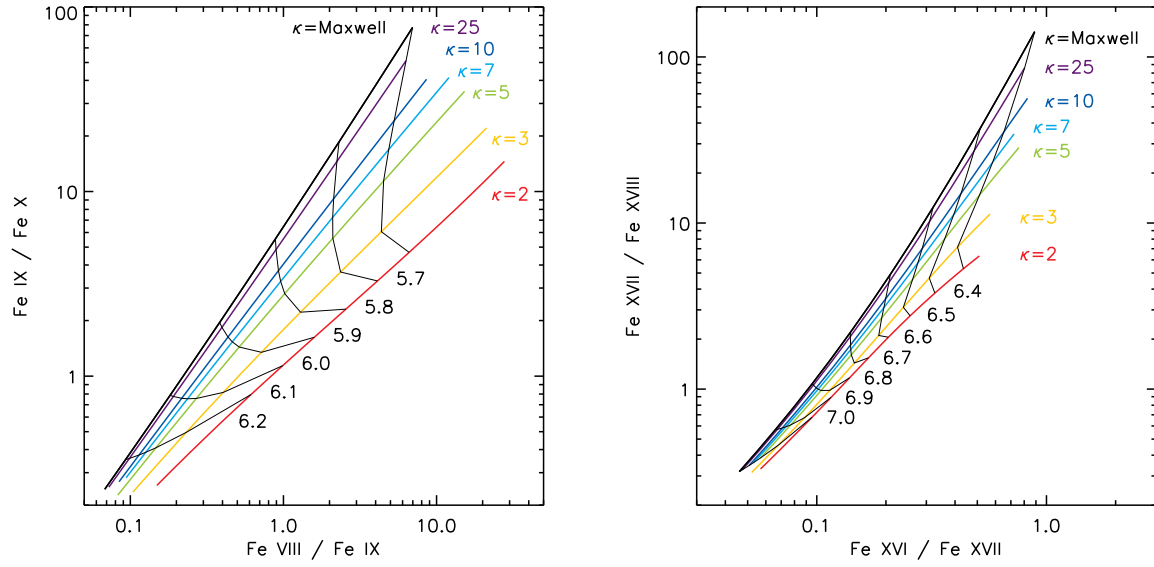


Figure 6. Diagnostics of κ from ratios of ion abundances. The values of κ for each line are indicated. Thin lines represent isotherms for the given value of $\log(T/K)$. (A color version of this figure is available in the online journal.)